Available online at www.sciencedirect.com

ScienceDirect

Procedia CIRP 82 (2019) 65–70

www.elsevier.com/locate/procedia

17th CIRP Conference on Modelling of Machining Operations

Evaluation of different flow stress laws coupled with a physical based ductile failure criterion for the modelling of the chip formation process of Ti-6Al-4V under broaching conditions

G. Ortiz-de-Zarate[a]*, A. Sela[a], F. Ducobu[b], M. Saez-de-Buruaga[a], D. Soler[a], T. H. C. Childs[c], P. J. Arrazola[a]

[a]*Mondragon Uniberstitatea, Faculty of Engineering, Loramendi 4, Arrasate-Mondragón, 20500, Spain*
[b] *University of Mons (UMONS), Faculty of Engineering (FPMs), Machine Design and Production Engineering Lab 7000 Mons, Belgium*
[c] *School of Mechanical Engineering, University of Leeds, Leeds LS29JT, UK*

* Corresponding author. Tel.: +34 943 79 47 00; fax: +34 943 79 15 36. *E-mail address:* gortizdezarate@mondragon.edu

Abstract

During the machining of Ti-6Al-4V the changing deformation mechanisms produce a complex microstructure of segmented chips, which directly influenced tool-wear and process stability. Numerical simulation could give an insight into the physical phenomena involved in chip segmentation, but its accuracy is directly related to the reliability of the input parameters. In this work, therefore, three different flow stress law were evaluated coupled with a physical based ductile failure criterion, which depends on stress triaxiality and temperature. To this end, the flow stress laws were implemented in the finite element software AdvantEdge by programming user-defined subroutines. The resulting FEM models were compared with orthogonal cutting experimental tests (tubular/linear), analyzing different fundamental outputs (machining forces, temperatures in the workpiece and chip morphology). All the FEM models showed good agreement with the experimental results.

Peer-review under responsibility of the scientific committee of The 17th CIRP Conference on Modelling of Machining Operations

Keywords: FEM; machining; Ti-6Al-4V; orhtogonal cutting; broaching

1. Introduction

In recent years, titanium alloys have received considerable interest due to their wide range of applications mainly in the aerospace, automotive, chemical and medical industries. Ti-6Al-4V (Ti64) is the most widely used titanium alloy that accounts more than 50% of the total titanium alloy production [1]. It presents low density in combination with high strength at significantly elevated temperatures, as well as, high creep and corrosion resistance [2]. Nevertheless, these thermomechanical properties mean this alloy is considered difficult-to-cut material mainly on account of its poor machinability resulting from its low thermal conductivity and high chemical activity.

These properties at certain cutting conditions may produce chip segmentation [1], [3]. At high cutting speeds, it is commonly believed that the only reason for chip segmentation is adiabatic shearing, produced by the thermal softening of the primary shear zone [4], [5]. However, at low cutting speeds researchers have also reported the appearance of segmented chips. They argue this is due to the lack of ductility of the material which results in ductile failure and consequently chip segmentation [3], [6], [7].

In machining conditions where segmented chip is obtained, significant force fluctuation occurs due to the change in the shear angle [8]. That fluctuation is commonly believed to be harmful to cutting tool life, because it causes fatigue damage to the tool and poor surface integrity of the machined part [1], [4],

2212-8271
Peer-review under responsibility of the scientific committee of The 17th CIRP Conference on Modelling of Machining Operations
10.1016/j.procir.2019.04.067

[8]. However, few works are reported in literature analyzing the chip segmentation phenomenon produced by the lack of ductility of the material.

Broaching is a machining operation where low cutting speeds are commonly used. In such machining operations, lack of ductility is the main reason for chip segmentation which can produce severe degradation of the tool. In this scenario, the Finite Element Method (FEM) could give an insight into the physics involved in chip segmentation, and thus help improve tool design. Using this approach has the benefit of reducing the number of trial and error experimental tests, which is of special interest in this machining operation due to the high manufacturing cost of the broaching tools.

However, for the development of accurate finite element models it is necessary to select the adequate input parameters in order to obtain robust results. As reported by Arrazola et al. [9] and Melkote et al. [10] the flow stress law is one of the key input parameters for FEM models. Moreover, Childs et al. [3] observed that in the prediction of chip segmentation the selection of the proper ductile failure model also significantly influenced the accuracy of the results.

This paper focuses on the evaluation of three different flow stress laws coupled with a physical based ductile failure model for the prediction of fundamental variables (forces, temperatures in the workpiece and chip morphology) when orthogonal cutting titanium alloy Ti64 in conditions close to broaching. To this end, experimental compression tests were carried out at different conditions, varying the strain rate and temperature. Then, the results were adjusted to the different flow stress laws (Johnson and Cook, Power Law and Iturbe et al. [11]). Afterwards, the flow stress laws and the ductile failure criterion were implemented in the Finite Element software AdavantEdge by user-defined subroutines. Finally, the predicted results were compared to experimental orthogonal/linear cutting tests.

2. Experimental tests

Orthogonal/linear cutting experimental tests were carried out in a Lagun CNC milling machining center (CNC 8070). The toolholder was set in the spindle, while the workpiece was fixed to a force measurement dynamometer (Kistler 91299AA). The dynamometer was clamped to the machine table, which transmitted a linear movement to the workpiece. The accuracy of the dynamometer is 0.3% for the forces on the three axes. The insert support has a resonant frequency of 160 Hz in the cutting direction and 150 Hz in the thrust direction. The values were obtained by a hammer impact test, measuring the insert vibration with a laser displacement meter (resolution 0.01 μm). Fig. 1 shows the set-up.

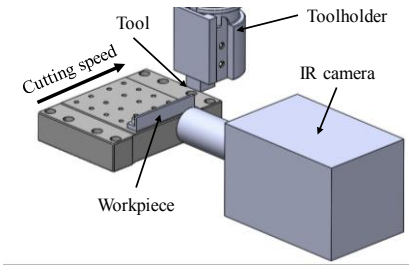

Fig. 1. The experimental set-up.

The titanium alloy Ti64 workpiece had a length of 90 mm, to ensure that the thermal steady state was reached during the linear cutting tests. This enabled the correct measurement of temperatures with the IR camera.

Broaching tools are generally made from High Speed Steel (HSS) because of the ease of manufacturing of this material. In the present research however, carbide inserts were employed as there is emerging interest in the development of broaching tools with interchangeable inserts, which could increase productivity, primarily in roughing conditions [12].

The cutting condition selected (cutting speed of 7.5 m/min and feed of 0.1 mm) was close to those found in roughing broaching. Table 1 shows the input parameters of the experimental tests.

Three trials were carried out to ensure robust results and estimate the uncertainty. All tests were performed in stable conditions without chatter or other phenomena that could affect the stability of the process. Moreover, the dynamics of the machine-tool were analysed by using the internal close-loop of the CNC to ensure that the whole linear test was carried out at a stable cutting speed with a deviation from the nominal cutting speed of less than 1%.

Table 1. Input parameters of the experimental tests.

Machine-tool	Type	High Speed Machining Center Lagun
Cutting tool	Insert reference	Sandvik-TPUN 160312 H13A
	Material	Cemented carbide
	Coating	No
	Rake angle (º)	6*
	Relief angle (º)	5*
Toolholder	Reference	WIDIA CTFPR-2020K16
Lubrication	Type	Dry
Workpiece	Material	Ti64
	Width (mm)	2
	Length (mm)	90
Cutting conditions	Operation	Linear/orthogonal cutting
	Cutting speed (m/min)	7.5
	Feed (mm)	0.1

* The angles are after the positioning of the insert in the toolholder.

From each experimental test three output variables were analysed: (i) machining forces, (ii) temperatures in the workpiece and (iii) chip morphology. The equipment used for the acquisition of those variables is presented in Table 2. The measured forces were normalized by the width of cut (N/mm) to be comparable with the predictive models.

The chips were ground and polished to obtain the chip morphology in the middle of the width of cut. They were also chemically etched with Kroll – composed of 2 ml of HF (hydrofluoric acid), 4 ml of HCl (hydrochloric acid) and 100 ml of distilled water – to allow observation of the microstructure.

Table 2. Output parameters of the experimental tests.

Machining forces	Kistler 91299AA
Chip morphology	Leica DM IRM microscope
Temperatures	IR camera FLIR Titanium 550M

The temperature was measured in the workpiece by thermography using the IR camera FLIR Titanium 550M. This technique consists of recording radiations emitted in the infrared domain, where spectral radiance is the highest. The emitted radiation of a real object is characterized by emissivity, defined as the ratio between the radiance of the object to that of the black body, for identical viewing conditions and temperature. The characterization of emissivity is therefore necessary to obtain reliable results. However, if the measurement region is painted completely black, to approximate a black body, the emissivity could be set at close to 1. This is the methodology that was followed for the temperature measurements in this research.

3. FEM model

The adequate selection of input parameters is of key importance when developing FEM models. Therefore, in this section the analyzed flow stress models are presented, as well as the physical based ductile failure criterion. Finally, the general description of the FEM model is set out.

3.1. Flow stress model

For the thermo-mechanical characterization of the Ti64, compression tests were carried out by varying the strain rate and temperature to assess their influence on the flow stress of the material. The experimental tests were performed in a Gleeble 3500 for strain rates between 1 and 100 s^{-1} and temperatures between 20 and 1000ºC. Three tests were done for each condition to ensure the robustness of the results.

Three different flow stress models were analyzed in this research. The first was the Johnson and Cook model (JC) [13], due to its wide application in the machining numerical simulation field. The model considers isotropic hardening, strain rate hardening and thermal softening as three independent phenomena.

The Power Law (PL) applied by Childs et al. [3] for the prediction of fundamental variables in the machining of Ti64 was also analyzed. Like the JC model, this law also considers the influence of strain rate and temperature as independent terms. In addition, it introduces a cut-off strain to represent the strain softening, which the JC model does not consider.

Table 3. Adjusted flow stress model parameters.

JC		PL [3]		Iturbe	
A (MPa)	1130	σ_0 (MPa)	930	σ_s (MPa)	1400
B (MPa)	530	n	0.14	σ_0 (MPa)	1150
C	0.0165	c_1	-1.4 10^{-3}	A (MPa)	124.1
n	0.39	c_2	7.8·10^{-7}	n	0.17
$\dot{\varepsilon}_0$	1	m	0.03	r	16.19
T_{melt} (ºC)	1650	T_c (ºC)	600	m	0.005
T_{room} (ºC)	20	T_{melt} (ºC)	1650	B	549.4
m	0.61	ε_0	0.022	C	0.02
		$\dot{\varepsilon}_0$	0.015	D	1.003
				$\dot{\varepsilon}_0$	1

Finally, the flow stress model proposed by Iturbe et al. (Iturbe) [11] was evaluated. This last model is the most complex one since it includes a strain softening term, as well as coupling between strain rate and temperature. However, its application for the numerical modelling of the machining process has hardly been studied to date.

The adjusted parameters of the flow stress laws are presented in Table 3. The values of the PL were previously published in the work of Childs et al. [3].

Fig. 2 shows a comparison between the flow stress curves obtained with the three different models and the compression experimental tests. Different testing condition results are presented in order to show the veracity of the models at different conditions. All the models showed good correlation with the experimental tests and the trends were accurately predicted. The Iturbe model appears to obtain the best fit with the experimental results, followed by JC and PL. The greatest divergence between models were reported at high strains due to the difference in the strain hardening/softening term.

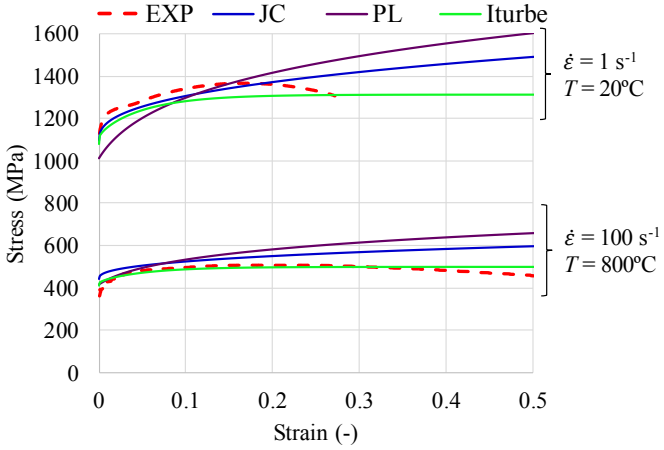

Fig. 2. Comparison between flow stress models and experimental results.

3.2. Ductile failure model

As explained in the introduction, it is necessary to introduce a ductile failure model to represent the chip segmentation phenomena observed in machining of titanium alloy Ti64 at low cutting speeds. The applied physical based ductile failure model was explained in detail by Childs et al. [3]. It allows the representation of the physics involved in chip segmentation for high and low cutting speeds. At low cutting speeds, such as those used in this research, the ductile failure governs the complete segmentation of the chip. At high cutting speeds, however, there is another failure mechanism, thermal softening, which causes adiabatic shearing in the primary shear zone.

Thus, the implemented ductile failure model consists of two stages: (i) initiation of the failure and (ii) flow stress reduction due to the failure of the workpiece material.

As regards failure initiation, the Mohr-Coulomb failure law was selected. This model consists of the accumulation of damage (D) along a streamline. The damage is a function of stress triaxiality (η) and failure coefficients ($\varepsilon_{f,0}$ and c) (equation 1). The onset of failure occurs when the damage value reaches 1.

$$D = \int_0^{\bar{\varepsilon}_f} \frac{d\bar{\varepsilon}}{\bar{\varepsilon}_f} \qquad (1)$$
$$\bar{\varepsilon}_f = \varepsilon_{f,0}\exp(c\eta)$$

To introduce the influence of temperature, which is known to affect ductile failure [14], [15], equation 2 was used. The values chosen for the ductile failure were obtained from the work of Childs et al. [3].

$$\begin{aligned} (\varepsilon_{f,0})_T &= \varepsilon_{f,0}(1 + aT), \quad T < T_{crit} \\ (\varepsilon_{f,0})_T &= \infty, \qquad\qquad T > T_{crit} \end{aligned} \qquad (2)$$

The influence of failure in the flow stress was presented as a reduction of the original flow stress as a function of the accumulated damage (D) and temperature [3].

3.3. Model description

The simulations were performed in the commercial machining finite element software AdvantEdge™-2D V7.4015. This software has a coupled thermo-elasto-plastic Lagrangian code with continuous remeshing and adaptive meshing. The minimum element size in the simulation was set to 2 µm to obtain accurate results. Consequently, the elapsed simulation time using a 4-core parallel was approximately 8 hours.

The flow stress laws coupled with the ductile failure model were implemented in the software by user-defined subroutines programmed in Fortran language.

The thermal conductivity and heat capacity of the Ti64 and tool material (H13A) were obtained from literature [16]. However, the heat capacity of the tool was significantly reduced from the physical value, so as to reduce the time to reach the thermal steady state. This strategy was demonstrated by Arrazola et al. [17] and by Childs et al. [3].

The tool micro geometry was measured by an optical profilometer, Alicona IFG4. The setup included a polarized lens of 10x with a ring light to improve the quality of the captured profiles. The vertical resolution was of 200 nm, and lateral 2 µm. A cutting edge radius of 25±2 µm was measured in all the edges used in the experimental tests (3 edges).

Finally, the tool-chip contact friction law was chosen. As observed by Arrazola and Ozel [18] the friction model strongly influences the simulation results, mainly in the thermal fields. The applied friction law was a sticking-sliding model (equation 3). Rech et al. [19] found that the sliding velocity is inverse to the friction coefficient, and thus at the low cutting speeds of broaching operations high friction coefficients need to be applied. To that end, in the present simulations a μ value of 1 was chosen ensuring that most of the contact was governed by the sticking region as reported by Childs [20].

$$\tau = \min(\mu\sigma_n, \bar{\sigma}/\sqrt{3}) \qquad (3)$$

A summary of the input parameters of the FEM model is presented in Table 4.

Table 4. Input parameters of the FEM model.

Young's modulus (GPa)	Ti6Al4V	115
	Carbide	500
Poisson's ratio	Ti6Al4V	0.3
	Carbide	0.3
Conductivity (W/mºC)	Ti6Al4V	6.7
	Carbide	100
Heat capacity (MJ/m^3)	Ti6Al4V	2.3
	Carbide	0.1
Friction coefficient	μ	1
Cutting speed (m/min)		7.5
Feed (mm)		0.1
Rake angle (º)		6
Clearance angle (º)		5
Cutting edge radius (µm)		25

4. Results and discussion

This research focuses on the evaluation of different flow stress laws with ductile failure model for the prediction of fundamental variables (machining force, temperatures and chip morphology) under broaching conditions. To this end a comparison was made between the predictions obtained with each of the flow stress models and the experimental results.

4.1. Machining forces

In the experimental results fluctuation of forces were obtained due to the segmentation of the chip. In Fig. 3 the red dashed lines represent the peaks and valleys in the experimental forces, which matches the chip segmentation. In general terms, the three flow stress models presented good agreement with the experimental results, and the peak and valley experimental forces were qualitatively well predicted by all the models. Nevertheless, the JC model appears to slightly underestimate the forces in comparison to the other models, as also observed by Ducobu et al. [21] for certain JC parameters of Ti64.

The main difference between the flow stress models resides in the frequency of the segmentation, i.e., the distance between peaks or valleys of the forces. As can be observed, a similar frequency was obtained for Iturbe and JC models and slightly lower for the PL. This is evaluated in greater depth in the chip morphology results.

4.2. Temperatures

All the temperatures of the simulations were obtained at the same point in time within their respective simulations, just after the beginning of the shearing of the chip, after 1 mm of cut, and once the thermal steady state was completely reached.

As can be observed in Fig. 4 all the models presented similar thermal fields, showing the highest temperatures in the primary shear zone, mostly near the cutting edge. Temperatures of up to 400ºC were obtained with the JC model, and even higher with the Iturbe and PL.

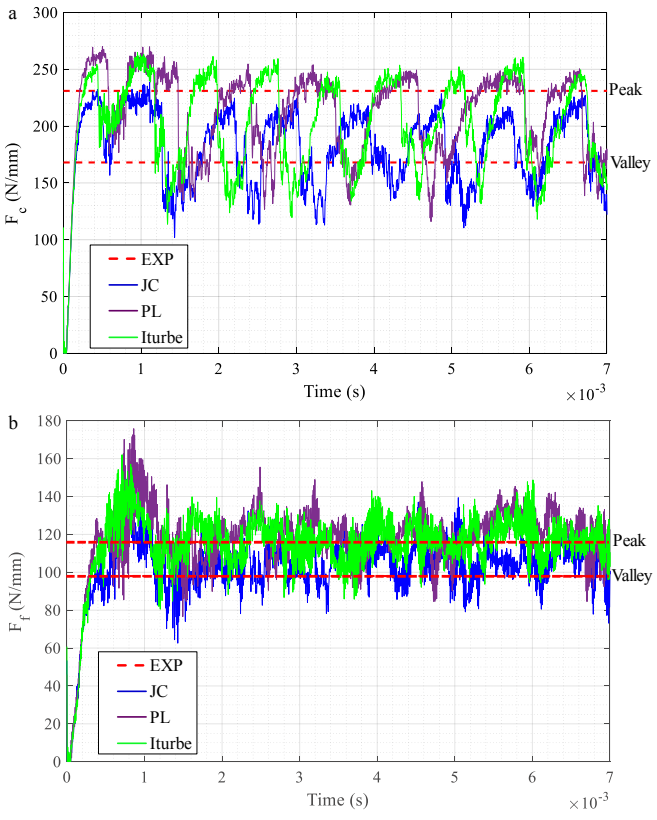

Fig. 3. Comparison between predicted and experimental machining forces.

When compared to the experimental results it can be observed that the temperatures in the chips were close to those of the primary shear zone (approximately 300ºC) in the experimental results, while in the FEM results the temperatures in the primary shear zones were 50-100ºC higher than in the chip.

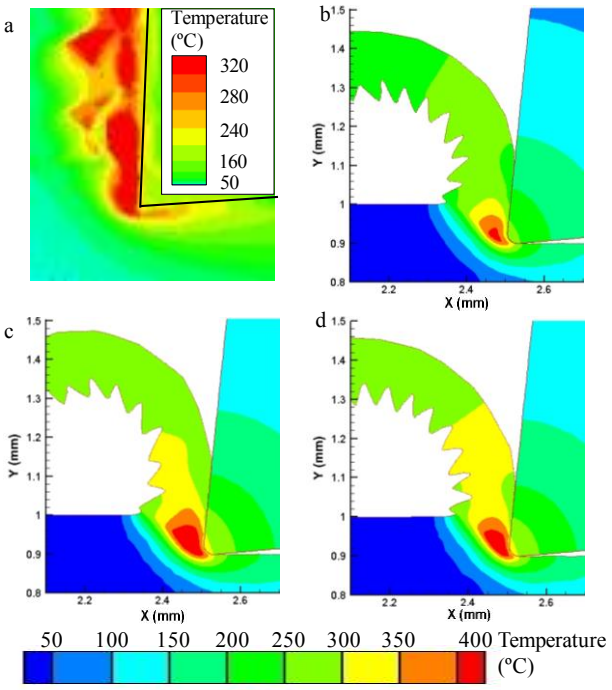

Fig. 4. Comparison between the temperatures obtained in the a) experimental results and FEM results with b) JC, c) PL and d) Iturbe models.

However, the uncertainty of the experimental tests, which could be about ±50ºC, needs to be taken into account. Moreover, in the FEM model the temperature of the middle of the width of cut is predicted while in the experimental tests it is measured lateral to the chip, which might report lower temperatures. The experimental characterization of the emissivity could also improve the accuracy of the experimental measurements.

Nevertheless, in general terms it could be stated that the three flow stress laws showed significantly good agreement with the experimental results.

4.3. Chip morphology

A comparison of both the experimental and FEM results is presented in Fig. 5. As can be observed, the predicted morphology qualitatively matches the experimental results. All the predicted chips presented similar plastic strain. The only visual difference is the segmentation frequency, since the pitch distance of the JC and Iturbe models appears to be lower than the PL, as was also observed in the machining force results.

To quantitatively analyze the accuracy of the FEM models a comparison was done between the predicted and the experimental results with regard to the peak, valley and pitch distances (see Fig. 6). All three models accurately predicted the analyzed variables. However, it must be noted that in the peak and valley prediction, the best agreement was obtained with the JC model, followed by PL and finally Iturbe.

Regarding pitch prediction, the Iturbe model showed the most accurate prediction, followed by JC and finally PL.

In general terms it could therefore be concluded that the JC model showed the best agreement with the experimental results regarding chip morphology prediction. Nevertheless, all the models were able to accurately predict chip morphology.

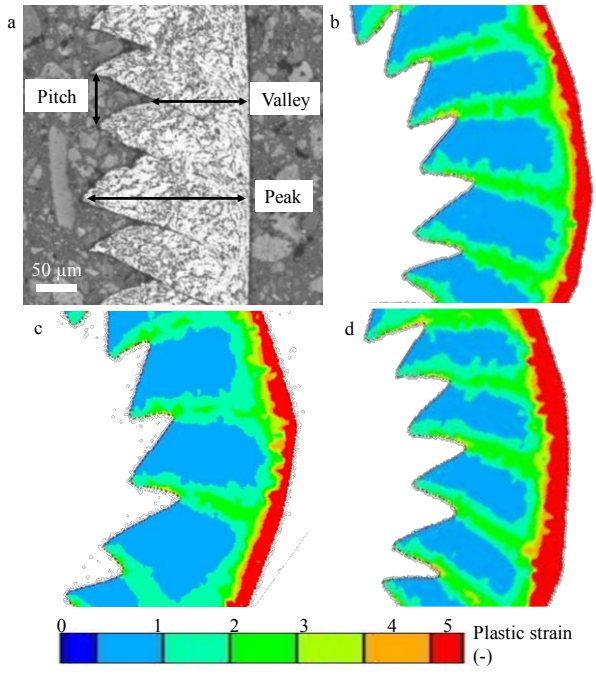

Fig. 5. Comparisons of chip morphology (all to the same scale) between a) experimental results and FEM results with b) JC, c) PL and d) Iturbe models.

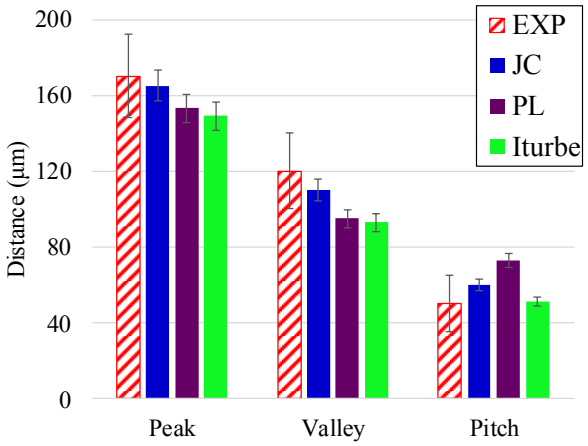

Fig. 6. Comparisons of chip morphology results.

5. Conclusions

In this paper, an evaluation of three different flow stress laws coupled with a physical based ductile failure model using FEM modelling has been presented. The main highlights of the study are the following:

- No significant differences were reported between the different flow stress models, with regards to the three analyzed fundamental variables (machining forces, temperature in the workpiece and chip morphology).
- All the prediction models showed good agreement with the experimental results for all outputs.
- Using complex flow stress models that take into account the strain softening phenomenon or/and the coupling between temperature and strain rate showed no significant improvement in the predictions.
- The reason for the small differences between models could reside in the cutting conditions. This is because the greater divergence between models are reported at high strain values, which are commonly produced in severe cutting conditions (high cutting speed and feed). Therefore, for broaching conditions where low cutting speeds are commonly used, the selection of a complex flow stress model seems not to have significant influence on the accuracy of the results.
- It is common practice to focus on experimental identification of the flow stress law, disregarding the ductile failure model. In the cases where ductile failure is considered, it is frequently obtained by a calibration procedure without any physical base. However, in the present work it has been demonstrated that the adequate selection of the ductile failure model could be a key aspect to accurately predict fundamental variables.

Acknowledgements

The authors hereby thank the Basque Government projects AEROBROCH (UE2016 - 07), SMAPRO (KK-2017/00021), MECAERO (PIBA 2018-85) and in the grant for Education and Training of Research Staff (PRE_2017_1_0394). The authors would also like to thank the Laboratory Technicians Denis Soriano and Erika Dominguez for their assistance in the realization of experimental tests and chip morphology analysis.

References

[1] P. J. Arrazola, A. Garay, M. Armendia, S. Marya, and F. Le Maitre, “Machinability of titanium alloys (Ti6Al4V and Ti555.3),” *Journal of Materials Processing Technology*, vol. 209, no. 5, pp. 2223–2230, 2009.
[2] R. M’Saoubi, D. Axinte, S. Leung, C. Nobel, H. Attia, G. Kappmeyer, S. Engin, and W. M. Sim, “High performance cutting of advanced aerospace alloys and composite materials,” *CIRP Annals*, vol. 64, no. 2, pp. 557–580, 2015.
[3] T. H. C. Childs, P. Arrazola, P. Aristimuno, A. Garay, and I. Sacristan, “Ti6Al4V Metal cutting chip formation experiments and modelling over a wide range of cutting speeds,” *Journal of Materials Processing Tech.*, vol. 255, pp. 898–913, 2018.
[4] R. F. Recht, “A Dynamic Analysis of High-Speed Machining,” *Journal of Engineering for Industry*, vol. 107, no. 4, pp. 309–315, 1985.
[5] J. Barry, G. Byrne, and D. Lennon, “Observations on chip formation and acoustic emission in machining Ti – 6Al – 4V alloy,” *International Journal of Machine Tool & Manufacture*, vol. 41, pp. 1055–1070, 2001.
[6] M. A. Elbestawi, A. K. Srivastava, and T. I. El-Wardany, “A Model for Chip Formation During Machining of Hardened Steel,” *CIRP Annals*, vol. 45, no. 1, pp. 71–76, 1996.
[7] M. C. Shaw and A. Vyas, “Chip Formation in the Machining of Hardened Steel,” *CIRP Annals-Manufacturing Technology*, vol. 42, no. 1, pp. 29–33, 1993.
[8] M. Cotterell and G. Byrne, “Dynamics of chip formation during orthogonal cutting of titanium alloy Ti – 6Al – 4V,” *CIRP Annals*, vol. 57, pp. 93–96, 2008.
[9] P. J. Arrazola, T. Özel, D. Umbrello, M. Davies, and I. S. Jawahir, “Recent advances in modelling of metal machining processes,” *CIRP Annals - Manufacturing Technology*, vol. 62, no. 2, pp. 695–718, 2013.
[10] S. Melkote, W. Grzesik, J. Outeiro, J. Rech, V. Schulze, H. Attia, P. J. Arrazola, R. M. Saoubi, and C. Saldana, “Advances in material and friction data for modelling of metal machining,” *CIRP Annals*, vol. 66, no. 2, pp. 731–754, 2017.
[11] A. Iturbe, E. Giraud, E. Hormaetxe, A. Garay, K. Ostolaza, and P. J. Arrazola, “Mechanical characterization and modelling of Inconel 718 material behavior for machining process assessment,” *Materials Science & Engineering A*, vol. 682, pp. 441–453, 2017.
[12] F. Klocke, P. Vogtel, S. Gierlings, D. Lung, and D. Veselovac, “Broaching of Inconel 718 with cemented carbide,” *Production Engineering*, vol. 7, no. 6, pp. 593–600, 2013.
[13] G. R. Johnson and W. H. Cook, “A constitutive model and data for materials subjected to large strains, high strain rates, and high temperatures,” *Proceedings of the 7th International Symposium on Ballistics*, vol. 21, pp. 541–547, 1983.
[14] G. R. Johnson and T. J. Holmquist, “Test data and computational strength and fracture model constants for 23 materials subjected to large strains, high strain rates, and high temperatures,” *Los Alamos National Laboratory Report LA-11463-MS*, 1989.
[15] J. T. Hammer, “Plastic deformation and ductile fracture of Ti-6Al-4V under various loading conditions,” The Ohio State University, 2012.
[16] A. Mondelin, F. Valiorgue, E. Feulvarch, J. Rech, and M. Coret, “Calibration of the insert/tool holder thermal contact resistance in stationary 3D turning,” *Applied Thermal Engineering*, vol. 55, no. 1–2, pp. 17–25, 2013.
[17] P. J. Arrazola, P. Aristimuño, D. Soler, and T. H. C. Childs, “Metal cutting experiments and modelling for improved determination of chip/tool contact temperature by infrared thermography,” *CIRP Annals*, vol. 64, no. 1, pp. 57–60, 2015.
[18] P. J. Arrazola and T. Özel, “Investigations on the effects of friction modeling in finite element simulation of machining,” *International Journal of Mechanical Sciences*, vol. 52, no. 1, pp. 31–42, 2010.
[19] J. Rech, P. J. Arrazola, C. Claudin, C. Courbon, F. Pusavec, and J. Kopac, “Characterisation of friction and heat partition coefficients at the tool-work material interface in cutting,” *CIRP Annals - Manufacturing Technology*, vol. 62, no. 1, pp. 79–82, 2013.
[20] T. H. C. Childs, “Ductile shear failure damage modelling and predicting built-up edge in steel machining,” *Journal of Materials Processing Technology*, vol. 213, no. 11, pp. 1654–1969, 2013.
[21] F. Ducobu, E. Rivière-Lorphèvre, and E. Filippi, “On the importance of the choice of the parameters of the Johnson-Cook constitutive model and their influence on the results of a Ti6Al4V orthogonal cutting model,” *International Journal of Mechanical Sciences*, vol. 122, pp. 143–155, 2017.